Chaos-Hyperchaos transition in three identical quorum sensing mean field coupled ring oscillators

N. Stankevich[1, a)] and E. Volkov[2, b)]
[1)] *HSE University, Nizhny Novgorod, 25/12 Bolshay Pecherskaya str., Nizhny Novgorod 603155, Russia*[c)]
[2)] *Department of Theoretical Physics, Lebedev Physical Institute, Moscow, 119991, Leninsky prospect, 53, Russia*

(Dated: 7 September 2021)

We investigate the dynamics of three identical three-dimensional ring synthetic genetic oscillators (repressilators) located in different cells and indirectly globally coupled by quorum sensing whereby is meant a mechanism in which special signal molecules are produced that, after the fast diffusion mixing and partial dilution in the environment, activate the expression of a target gene which is different from the gene responsible for their production. Even at low coupling strengths, quorum sensing stimulates the formation of a stable limit cycle, known in the literature as a rotating wave (all variables have identical waveforms shifted by one third of the period), which, at higher coupling strengths, converts to complex tori. Further torus evolution is traced up to its destruction to chaos and the appearance of hyperchaos. We hypothesize that hyperchaos is the result of merging the saddle-focus periodic orbit (or limit cycle) corresponding to the rotating wave regime with chaos and present considerations in favor of this conclusion.

With an increase in the number of unstable directions, multi-dimensional systems develop chaos and even hyperchaos characterized by two or more positive Lyapunov exponents. The key point in studying the hyperchaotic attractors is analysis of the chaotic attractor skeleton and the bifurcation mechanisms whereby attractors with multi-dimensional unstable manifolds are formed. One of the bifurcation giving rise to a saddle cycle with a two-dimensional unstable manifold is the Neimark-Sacker bifurcation, which leads to torus formation. Torus destruction via the Afraimovich-Shilnikov scenario generates chaos with one positive Lyapunov exponent. If the saddle cycle resulting from the Neimark-Sacker bifurcation is absorbed by a chaotic attractor, then hyperchaos may develop. This scenario was observed both in the dynamics of isolated and in coupled oscillators.

Here, we investigate the emergence of hyperchaos in a system of three identical ring oscillators (Repressilators) that are used to build synthetic genetic networks. The maximally reduced model of the isolated three-dimensional Repressilator of three genes demonstrates a smooth limit cycle over a wide range of model parameters. Repressillators embedded into different individual cells interact by the quorum sensing (QS) mechanism, in which signal molecules synthesized under the control of one of the genes quickly diffuse into a common environment and can take control of the expression of another gene in the ring. Such a scheme is realistic for genetic circuits and principally differs from linear diffusion of phase variables typically used in studies of collective regimes.

As known for the system of two identical Repressilators, QS interactions make possible the birth of inhomogeneous limit cycles (i. e. with different amplitudes), tori, and the emergence of large regions of parameters where chaos and multistability dominate. For three identical Repressilators we also use the QS scheme, in which weak coupling ensures the formation of a limit cycle in the form of a rotating wave. The evolution of the system with an increase in the coupling strength leads to the Neimark-Sacker bifurcation, which gives rise to a torus and turns the rotating wave cycle into a saddle-focus cycle with a two-dimensional unstable manifold. Then, torus destruction produces chaos, which turns into hyperchaos after merge with the saddle-focus cycle.

I. INTRODUCTION

Hyperchaos has been the subject of research for long time and many routes to its formation has been discovered. Starting from the famous paper[1], many successful attempts to get hyperchaos in isolated four-dimensional dynamical systems have been realized due to adding at least one variable to classical Rössler, e.g.[1,2], and Lorenz e.g.[3,4] systems. Several autonomous hyperchaotic oscillators were not only investigated using bifurcation analysis but realized in electronic circuits[5,6]. In recent works[7,8] it has been shown that hyperchaos appears in the modified four-dimensional Anishchenko-Astakhov generator.

Other examples of hyperchaos emergence have been found during the studies of coupled systems. In particular, coupled chaotic oscillators demonstrate hyperchaos: in the ring of Chua's circuits[9]; in two Rössler's oscillators coupled by linear diffusion of one variable[10–12]; in Colpitts oscillators coupled by means of two linear resistors[13]. Hyperchaos was demonstrated via numerical simulations and hardware experiments: bi-directional non-linear coupling, symmetric with respect to

[a)]Electronic mail: stankevichnv@mail.ru.
[b)]Electronic mail: volkov@td.lpi.ru
[c)]Also at Department of Radio-Electronics and Telecommunications, Yuri Gagarin State Technical University of Saratov, 77 Politekhnicheskaya str., Saratov 410054, Russia.; Also at Department of Applied Cybernetics, St. Petersburg State University, Saint-Petersburg, Peterhof, 28 Universitetskiy proezd, St. Petersburg 198504, Russia

the state variables, results in the appearance of hyperchaos in two identical Chua's circuits[14].

There are publications in which hyperchaos arises in coupled regular oscillators stimulated by external periodic oscillation. For example, in the well-known paper[15] it has been shown that two directly linearly coupled van der Pol oscillators under the same common periodic stimulation demonstrate hyperchaos among as one of the other attractors. Recently chaos and hyperchaos have been found in coupled antiphase driven Toda oscillators[16]. In[16] three possible routes to hyperchaos were discussed. One of them (for weak coupling strength) related to the scenario which was observed for coupled chaotic systems. Driven Toda oscillator is well-known example of a model demonstrating transition to chaos via cascade of period-doubling bifurcations at increasing of external force amplitude. For stronger coupling strength another scenario of hyperchaos occurrence was observed associated with torus destruction. Last scenario was discussed in[7,8] for the simplest four-dimensional autonomous model of radiophysical generator[17] and model of two interacting microbubble contrast agents under ultrasound stimulation[18]. It was shown that torus destruction can lead to formation of discrete Shilnikov's chaotic attractor as a result of absorption of saddle cycle with two-dimensional unstable manifold appeared at torus birth[19–21]. Saddle cycle with two-dimensional unstable manifold contributes to chaotic attractor leading to hyperchaos.

Other route to hyperchaos has been investigated in the ring of unidirectionally coupled identical Duffing oscillators which are in stable steady state without coupling. Detailed analysis of dynamics in the presence of linear cross-diffusion has demonstrated a classical cascade: periodic, quasiperiodic, chaotic and hyperchaotic attractors partially verified in a simple electronic experiment[22].

We assume that it would be important to consider other types of simple regular oscillators and new types of coupling schemes that provide the interesting route to hyperchaos formation. Here we explore long known the three-dimensional ring oscillator which attracted attention after its realization in the form of real synthetic genetic circuit implemented in bacteria under name "Repressilator"[23–25]. We use the simplest version of Repressilator constructed from three genes, a, b and c, which negatively regulate each other's transcription in a cyclic fashion, namely a regulates b, b regulates c and c regulates a (see Fig. 1a). The regulation is performed by the transcription factors, or repressors, A, B and C, coded by genes a, b and c, respectively. The first mathematical model demonstrating oscillation in this circuit has been presented already in[23] followed by publications with rigorous mathematical analysis[26,27]. Repressilator's limit cycle remains stable over very large areas of its control parameters and does not demonstrate period doubling bifurcations.

Synthetic genetic oscillators are very important motif for genetic engineering and in many applications the effectiveness of oscillations strongly depends on the collective modes they can form to escape averaging of oscillations in population of cells with oscillators inside.

Soon after publications on different genetic oscillators, the "quorum sensing" mechanism of bacterial communication has been suggested to couple them[28,29]. Bacterial quorum sensing (QS) which provides for communications in bacterial populations by fast diffusion of small specific molecules (autoinducers), is a natural candidate for the role of being a manager for synthetic genetic network dynamics. This idea was effective, for instance, in constructing several synthetic multicellular systems like the ecological predator-prey[30], population control[31], and other models (see references in a review[32]). Interesting examples of the QS-stimulated synchronization of population of real genetic clocks[33] and of modeled biologically plausible coupled circuits have been published during the last decade[34].

In 2007, another version of the QS mechanism was integrated into the 6-dimensional Repressilator model[35]. Studies of two coupled identical Repressilators revealed very complex dynamics in significant areas of control parameters[36–38]. Weakly coupled repressilators oscillate in antiphase and this limit cycle loses stability via Neimark-Sacker bifurcation. With the increasing coupling strength, the formation of a rich family of resonant cycles with different winding numbers is observed. In addition, an unexpected strongly inhomogenous limit cycle arises which is not only stable over a wide domain of parameter plane but also can coexist with symmetric attractors. Its stability is ruled by period-doubling or Neimark-Sacker bifurcations, which leads to chaos.

At the expense of chaotization, the symmetry of time series tends to restore in the form of generation of random alternations of time intervals with asymmetric pieces, which reflects the domination of the chaos framework by unstable inhomogeneous periodic orbits (UPO) in certain parameter areas. Interestingly, despite the demonstration of rich multistability, chaotization of different regimes and the presence of many UPO in 8-dimensional phase space of two Repressilators, no manifestation of hyperchaos was detected in the parameter space studied.

Recently, we have considered torus evolution as a function of the coupling strength for three QS-coupled Repressilators and detected some precursors of hyperchaos[39]. However, the control parameter of the transcription rate was varied only in a limited range. Here we extend the area of control parameters to study the transition from chaos to hyperchaos in more detail by scanning the parameter plane and computing the spectrum of Lyapunov exponents. A large region was found where hyperchaos is clearly seen.

For three coupled identical Repressilators we start analysis with the stable limit cycle corresponding to the rotating wave regime (RW). It loses stability via Neimark-Sacker bifurcation which leads to the appearance of two-frequency torus. To clarify the mechanism of hyperchaos formation we traced tori's evolution and destruction into chaos and the following chaos evolution with the increasing coupling strength. Then, the distance between unstable RW cycle and chaotic attractor was calculated and the critical value of coupling strength for merging saddle-focus limit cycle (RW) with chaos was determined. Their merge initiates hyperchaos formation.

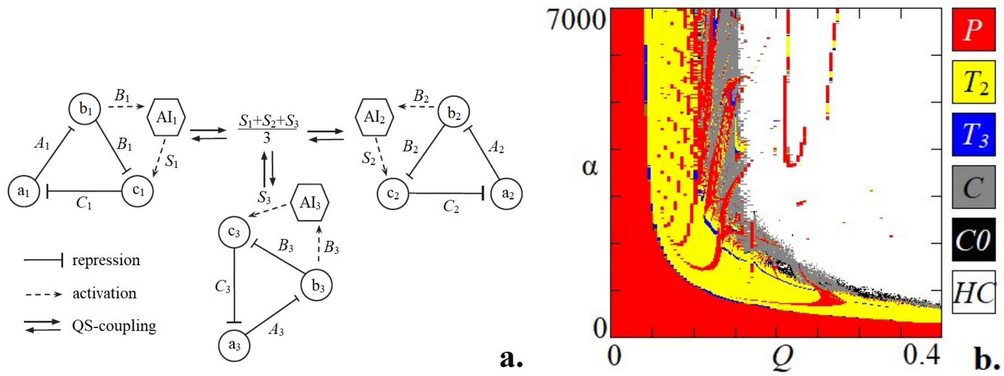

FIG. 1. **a.** Principle scheme of three quorum-sensing coupled Repressilators. A_i, B_i, C_i are proteins in each Repressilators; a_i, b_i, c_i are mRNAs produced by three genes; AI$_i$ are autoinducers and S_i are their concentrations. **b.** Chart of regimes revealed by values of Lyapunov exponents for model (1). The steps of parameters during scanning are: $h_Q = 0.001$, $h_\alpha = 23$. P is periodic oscillations (red), T2 is two-frequency quasiperiodic oscillations (yellow), C, $C0$, HC are chaotic regimes with different signatures of Lyapunov exponents spectrum (grey, black, white)

II. OBJECT OF INVESTIGATION AND METHODS

As the basis we use a reduced version of the model described earlier (see[36–38] for details) and adapted for three three-dimensional Repressilators coupled via autoinducer production and diffusion. Figure 1 shows three Repressilators located in different cells (or other appropriate containers impermeable to repressors) and coupled via QS exchange with the external medium. The three genes in the ring produce mRNAs (a, b, c) which are translated to proteins (A, B, C), and they impose Hill function inhibition on each other in a cyclic order by the preceding gene. The QS feedback is maintained by the AI produced (rate k_{S1}) proportionally to the protein B concentration while the autoinducer (AI) communicates with the environment and activates (rate κ in combination with Michaelis function) the production of mRNA for protein C, which, in turn, reduces the concentration of protein A, which results in the activation of protein B production. In this way protein B plays a dual role of direct inhibition of protein C synthesis and AI-dependent activation of protein C synthesis, resulting in complex dynamics of the Repressilator, even for a single Repressilator[40]. The resulting equations for dimensionless repressors (A, B, C) and autoinducer (S) concentrations are:

$$\begin{aligned}
\dot{A}_i &= \beta_1(-A_i + \tfrac{\alpha}{1+C_i^n}),\\
\dot{B}_i &= \beta_2(-B_i + \tfrac{\alpha}{1+A_i^n}),\\
\dot{C}_i &= \beta_3(-C_i + \tfrac{\alpha}{1+B_i^n} + \tfrac{\kappa S_i}{1+S_i}),\\
\dot{S}_i &= -k_{S0}S_i + k_{S1}B_i - \eta(S_i - S_{ext}),
\end{aligned} \tag{1}$$

where $i = 1,2,3$ are subscripts for the three Repressilators, β_j ($j = 1,2,3$) are the ratios of the protein decay rate to the mRNA decay rate, α stands for the maximum transcription rate in the absence of the inhibitor, and n is the Hill cooperativity coefficient for inhibition. For the quorum sensing pathway k_{S0} is the ratio of the S decay rate to the mRNA decay rate, and as previously mentioned, k_{S1} is the rate of production of S: κ gives the strength of S-dependent activation of protein C production. The diffusion coefficient η depends on the membrane permeability to the S molecule. The concentration of S in the external medium S_{ext} is determined (in a quasi-steady state approximation) by S produced by all the Repressilators (S_1, S_2, S_3) and a dilution factor Q:

$$S_{ext} = Q\frac{S_1 + S_2 + S_3}{3}. \tag{2}$$

The model parameters are fixed identical for each Repressilator and close to what was proposed in[41]: $\beta_1 = 0.5$, $\beta_2 = \beta_3 = 0.1$, $n = 3$, $k_{S0} = 1$, $k_{S1} = 0.01$, $\eta = 2$, $\kappa = 15$. As a control parameter, we use the coupling strength Q and the maximum transcription rate in the absence of inhibitor α.

When $Q = 0$ each of the oscillators is a self-sustained element. The amplitude of the limit cycle is regulated by the parameters α, β. With a small coupling in the ensemble (1), the so-called rotating wave (RW) solution is observed, when the time series of each repressor are the same, but are shifted relative to each other by a third of the period. Increasing of the coupling Q and amplitude leads to a complication of the dynamics. Analysis and classification of possible types of dynamics can be carried out using the spectrum of Lyapunov exponents. Figure 1b shows a chart of the Lyapunov exponents of the model (1), on which the colors indicate areas of different dynamics depending on the values of the Lyapunov exponents. Lyapunov exponents were calculated using the algorithm proposed in[42]. The value $\varepsilon = 10^{-4}$ was used as the threshold value for determining zero. The following types of behavior are classified:

- periodic oscillations (P), red color, $\Lambda_1 = 0$, $0 > \Lambda_2 > \Lambda_3 > \Lambda_4 > \Lambda_5 > \Lambda_6 > \Lambda_7 > \Lambda_8 > \Lambda_9 > \Lambda_{10} > \Lambda_{11} > \Lambda_{12}$;
- two-frequency quasiperiodic oscillations (T_2), yellow

color $\Lambda_1 = \Lambda_2 = 0,\ 0 > \Lambda_3 > \Lambda_4 > \Lambda_5 > \Lambda_6 > \Lambda_7 > \Lambda_8 > \Lambda_9 > \Lambda_{10} > \Lambda_{11} > \Lambda_{12}$;

- three-frequency quasiperiodic oscillations or points near torus doubling bifurcations (T_3), blue color $\Lambda_1 = \Lambda_2 = \Lambda_3 = 0,\ 0 > \Lambda_4 > \Lambda_5 > \Lambda_6 > \Lambda_7 > \Lambda_8 > \Lambda_9 > \Lambda_{10} > \Lambda_{11} > \Lambda_{12}$;

- chaotic oscillations (C), grey color, $\Lambda_1 > 0,\ \Lambda_2 = 0,\ 0 > \Lambda_3 > \Lambda_4 > \Lambda_5 > \Lambda_6 > \Lambda_7 > \Lambda_8 > \Lambda_9 > \Lambda_{10} > \Lambda_{11} > \Lambda_{12}$;

- hyperchaotic oscillations (HC), white color, $\Lambda_1 > \Lambda_2 > 0,\ \Lambda_3 = 0,\ 0 > \Lambda_4 > \Lambda_5 > \Lambda_6 > \Lambda_7 > \Lambda_8 > \Lambda_9 > \Lambda_{10} > \Lambda_{11} > \Lambda_{12}$;

- chaotic oscillations characterized by an additional zero Lyapunov exponent in the spectrum ($C0$), black color, $\Lambda_1 > 0, \Lambda_2 = \Lambda_3 = 0,\ 0 > \Lambda_4 > \Lambda_5 > \Lambda_6 > \Lambda_7 > \Lambda_8 > \Lambda_9 > \Lambda_{10} > \Lambda_{11} > \Lambda_{12}$.

The chart shown in Fig. 1b was constructed by scanning the parameter plane with adiabatic initial conditions and increasing in the parameter α: we take fixed initial conditions for each new value of Q at $\alpha = 0$ corresponding to limit cycle RW-solution and then for each new value of α we take initial conditions from last step of previous α. Such calculations do not give a complete analysis of the dynamics but show the general layout of the mode map for further detailed study. The three-frequency quasiperiodic regime T_3 and chaos with additional Lyapunov exponent $C0$ revealed by scanning are stable over very narrow parameter intervals. They are not essential for hyperchaos formation.

The analysis of the structure of the parameter plane shows that Neimark-Sacker bifurcation of the limit cycle corresponding to the rotating wave (RW) results in two-frequency quasiperiodic oscillations formation along the line crossed all considered parameter plane. For small coupling strength along the Neimark-Sacker bifurcation line, synchronization tongues are observed. The destruction of quasiperiodic oscillations leads to the formation of chaotic dynamics. Chaotic dynamics arises in a certain intervals of the coupling parameter, which become longer with an increase in the parameter α. The chaotic attractor then develops into a hyperchaos which dominates. Next, we will consider in more detail the mechanism of transformation of a chaotic attractor into a hyperchaotic one and the roles of various regimes in this process.

III. BASIC SOLUTIONS IN THREE COUPLED IDENTICAL SYSTEMS

Ashwin et al.[43] presented theoretical and experimental investigation of three identical oscillators with weak symmetric coupling and observed stable in-phase limit cycle and a stable rotating waves (RW). Three coupled chemical oscillators in a triangular arrangement demonstrated the following set of periodic regimes: three oscillators are running in-phase (InP), two in-phase oscillators out of phase with the third one (2in-1out) asymmetric limit cycle and RW, see e.g.[44]. A ring of three Fitzhugh-Nagumo-like relaxation oscillators coupled via diffusion of slow (recovery) variables can oscillate in-phase, in an RW regime and in asymmetric 2in-1anti limit cycle[45]. Numerical analysis and experiments with three electronic relaxation voltage-coupled oscillators show the successful persistence of the above-mentioned collective regimes in the presence of small detuning[46].

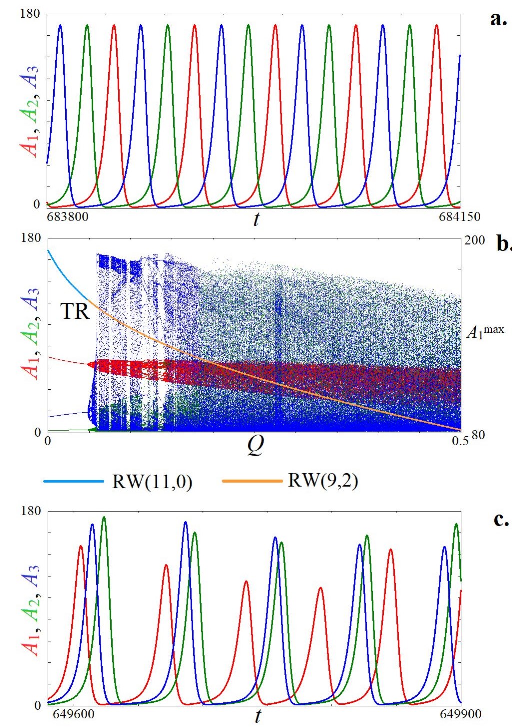

FIG. 2. Illustrations of trajectories in model (1): **a.** - stable rotating wave time series for $Q = 0.01$, $\alpha = 2777$; **b.** - bifurcation tree in cross-section by hypersurface $C_1 = 5.0$ for $\alpha = 2777$, shown along with Q-parameter AUTO continuation of stable RW (blue line) and unstable one (orange line); **c.** - time series for two-frequency torus, $Q = 0.1$, $\alpha = 2777$. (gaps in the tree picture are for the data still being computed).

The structure of Repressilators and the scheme of QS-coupling between them differ from those used in previous publications, which made it necessary to check the appearance of stable periodic regimes in the weakly coupled Repressilators.

For given intervals of model parameters the in-phase limit cycle is not stable because a repulsive tendency dominates the coupling[35,36]. The RW stability observed in our system (1) for $\alpha < 400$ (it was considered in[39]) takes place over all α considered (see Fig.1b); the time series of RW for $\alpha = 2777$ is depicted in Fig. 2a. The RW stability interval vs coupling strength is bounded by Neimark-Sacker bifurcation (TR) (see the bifurcation tree and Q-parameter bifurcation diagram of limit cycle RW obtained with help of AUTXPP software[47] in

Fig. 2b). The bifurcation tree is calculated using the cross-section by hypersurface $C_1 = 5.0$ and is presented as three same name dynamic variables of each repressilators (red, blue and green). AUTO-continuation demonstrates the maximum amplitude of the first variable A_1: light blue is a stable RW-solution RW(11,0); orange line, saddle solution RW(9,2). Scale for A_1^{max} is shown on the right; scale for A_i in Poincaré section by hypersurface $C_1 = 5$, on the left. These scales are also used in other Figures below. Indices (m, n) denote the stability type of cycles, with m being dimension of stable manifold, and n, of unstable manifold. After torus destruction the dynamics is non-regular (Fig. 2c) but still resembles the rotating wave solution, because the order of variables is retained and the phase shifts between oscillators do not strongly fluctuate.

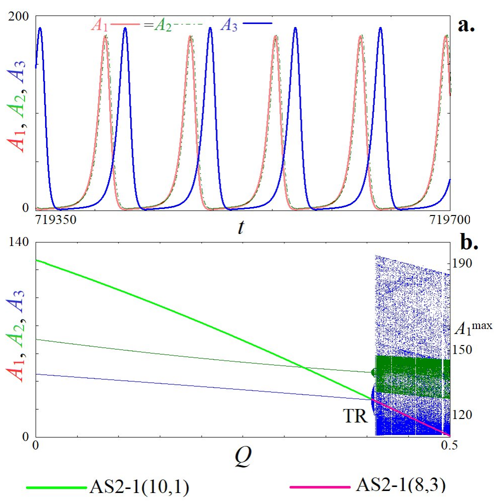

FIG. 3. Illustrations of 2in-1out 8-dimensional solution AS2in-1out for model (1) with winding number 1:1:1: **a.** - time series for $Q = 0.01$, $\alpha = 2777$; **b.** - bifurcation tree and AUTO continuation (light green (stable) and pink (unstable) lines) for $\alpha = 2777$.

The simplest way to determine the existence of asymmetric limit cycles is to choose identical initial phase points for two oscillators. Phase space reduction leads to detecting an 8-dimensional limit cycle (AS2in-1out(10,1)) with a winding number of 1:1:1. All asymmetric solutions (further we will show limit cycles AS2in-1out and AS3, torus, chaos) are formally 12-dimensional, but we will use expressions "8D cycle" and "8D chaos" because the equalization of phase variables of two oscillators effectively reduces 12-dimensional phase space to 8-dimensional. Time series of AS2in-1out(10,1) cycle are presented in Fig.3a. This cycle is invisible among regimes in Fig.1b calculated using 12-dimensional random initial points, because any perturbations of identity of two in-phase oscillators destroy AS2in-1out. Despite this specific fatal sensitivity, an increase in coupling strength results in bifurcation of cycle AS2in-1out (see Fig. 3b) which can be important for the general dynamics due to the appearance of 8-dimensional chaos at $Q = 0.4$. Further transformations of the cycle are associated with Neimark-Sacker bifurcation (TR) and Afraimovich-Shilnikov's scenario of torus destruction[48]. Notice that in this case we deal with the cycle that has one-dimensional unstable manifold AS2in-1out(10,1) and transforms to the cycle with three-dimensional unstable manifold AS2in-1out(8,3) via Neimark-Sacker bifurcation.

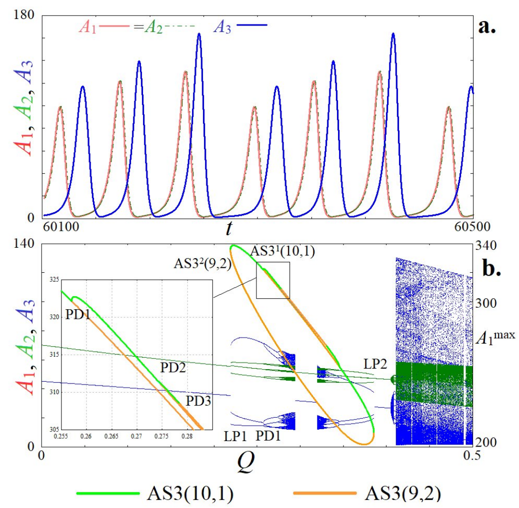

FIG. 4. Illustrations of 2-in-1-out 8-dimensional period-3 for model (1): **a.** - time series of AS3 for $Q = 0.22$, $\alpha = 2777$; **b.** - AUTO Q-continuation of AS3 cycle: stable (green) and unstable (red) limit regimes; bifurcation tree of the same cycle AS3 in interval LP1-LP2 and tree for AS1-2 after $Q > Q(LP2)$.

This eight-dimensional solution in the system (1) is not the only one. With an increase in coupling, for example, one can observe another asymmetrical saddle cycle of period three (AS3), for which two oscillators are completely synchronous, and the third one is in anti-phase with them (see Fig.4a). Fig. 4b shows the one-parameter AUTO continuation and bifurcation tree for this cycle as a function of Q. As a result of the saddle-node bifurcation at $Q = 0.2191$ (LP1), a pair of saddle cycles arises: one has a one-dimensional unstable manifold $AS3^1(10,1)$ (upper line of Q-continuation in Fig. 4b), and the other has a two-dimensional one $AS3^2(9,2)$ (lower part of Q-continuation). With an increase in coupling, cycle $AS3^1(10,1)$ undergoes a cascade of period doubling bifurcations starting from PD1 which transforms $AS3^1(10,1)$ into cycle $AS3^1(9,2)$ at $Q = 0.257$ (see inset in Fig. 4b). The cascade of period-doubling bifurcations leads to weak chaos which undergoes crisis at $Q \approx 0.295$.

The similar evolution of the dynamics is observed when we start from the right side of the period-3 region. The backward Q-continuation shows that at $Q = 0.3855$ saddle-node bifurcation (LP2) occurs giving rise to two cycles: $AS3^1(10,1)$ and $AS3^2(9,2)$. Cycle $AS3^1(10,1)$ transforms to chaos via period-doubling bifurcations and at $Q \approx 0.319$ the chaotic attractor disappears and the system goes to the 8-dimensional period-1 cycle AS2in-1out-1. Both cascades are illustrated in Fig. 4b as

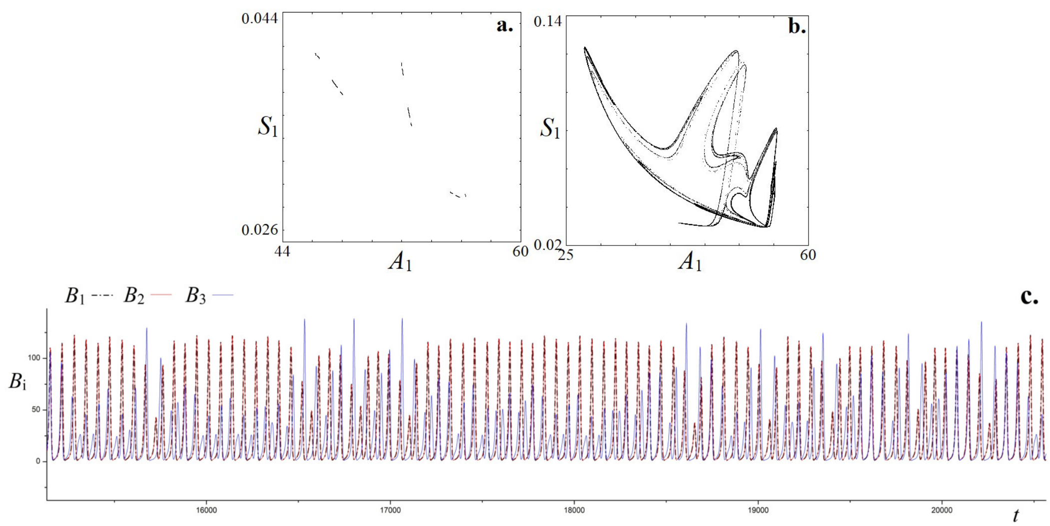

FIG. 5. Poincaré sections obtained by hypersurface $C_1 = 5.0$ for two types of 8D chaotic solutions: **a.** born via period-doubling bifurcations cascade of AS2in-1out cycle at $Q = 0.28$; **b.** born via destruction of torus born from cycle AS3 at $Q = 0.45$. **c.** Time series for 8D chaotic attractor, $Q = 0.45$.

AS3(10,1) AUTO continuation and bifurcation trees for AS3.

Interestingly, for $\alpha = 2777$ the chaotization of the cycle AS3 brings about a gap in its bifurcation tree. The crisis of AS3-dependent chaos may occur due to amplitude growth of chaotic trajectories so that they can cross the boundary of the basin of the dominant stable 8-dimensional cycle 2in-1out. Therefore, inside the gap the bifurcation tree is represented by only one line corresponding to the AS2in-1out cycle. The branch of the unstable cycle $AS3^2$(9,2) does not undergo bifurcations, it merges with $AS3^1$ as a result of saddle-node bifurcations LP1, LP2.

Thus, we show the presence of various solutions that can form the skeleton of a chaotic attractor and thereby determine the type of this attractor. Furthermore, we can see the formation of an 8D chaotic attractor, which also has its own skeleton. In Fig.5 two examples of chaotic attractors are presented. Fig. 5a and 5b give the Poincaré maps of the 8-dimensional chaotic saddle manifold. Fig.5a demonstrates chaos born via a cascade of period doubling bifurcations of saddle cycle of period-3 AS31. Another chaos presented in Figs. 5b, 5c emerges via Neimark-Sacker bifurcation of AS2in-1out period-1 cycle and destruction of the newly born saddle torus. In the next section, we consider the emergence of chaotic attractors, as well as the mutual arrangement of the cycles and their influence on the dynamics.

IV. HYPERCHAOS RESULTING FROM THE FORMATION OF THE SHILNIKOV'S ATTRACTOR

Fig. 1 clearly demonstrates the presence of hyperchaos over wide areas of parameters $Q-\alpha$. The amplitude of oscillations in our system (1) is mainly controlled by parameter α, the rate of repressors production. In[39] it was shown that at small α the detection of hyperchaos is unreliable due to very small values of positive Lyapunov exponents.

For $\alpha = 2777$ the evolution of hyperchaos is traced in detail (Fig. 6) via analysis of Poincaré maps for critical values of coupling strength where qualitative changes of Lyapunov exponents are observed (Fig. 6a).

Figure 6b shows an enlarged fragment of the graphs of the three largest Lyapunov exponents in the Q-region where the primary torus destruction and the formation of a chaotic attractor take place; marked are the basic bifurcations leading to chaos development. As can be seen from the graphs of Lyapunov exponents, the RW is well diagnosed (the largest exponent is close to zero, the next two are negative and equal to each other, and the fourth exponent is less than -0.02 and is not visualized in Fig. 6b). At $Q \approx 0.048$ Neimark-Sacker bifurcation (TR) leads to the two-frequency torus displayed in Fig. 6c. Then, we observe a sequence of saddle-node bifurcations (LP1, LP2, LP3), which are the boundaries of Arnold's tongues for resonant cycles. Undergoing this sequence of saddle-node bifurcations, the quasiperiodic regimes persist through it; however, they become more complex (Fig. 6d). For some intervals of parameters α and Q the evolution of the tori and the possibility of bistability between the two tori were preliminary considered in[49].

As a result of the saddle-node bifurcation (LP4), a resonance cycle of period 23 is born on the torus surface (Fig. 6e). After passing through resonant tongues, the maps become more complex and gradually becomes non-smooth approaching a collapse in accordance with the Afraimovich-Shilnikov scenario. Fig. 6f shows an example of a Poincaré map for the nonsmooth torus; Fig. 6g corresponds to a chaotic regime, which is characterized by one positive, one zero and 10 nega-

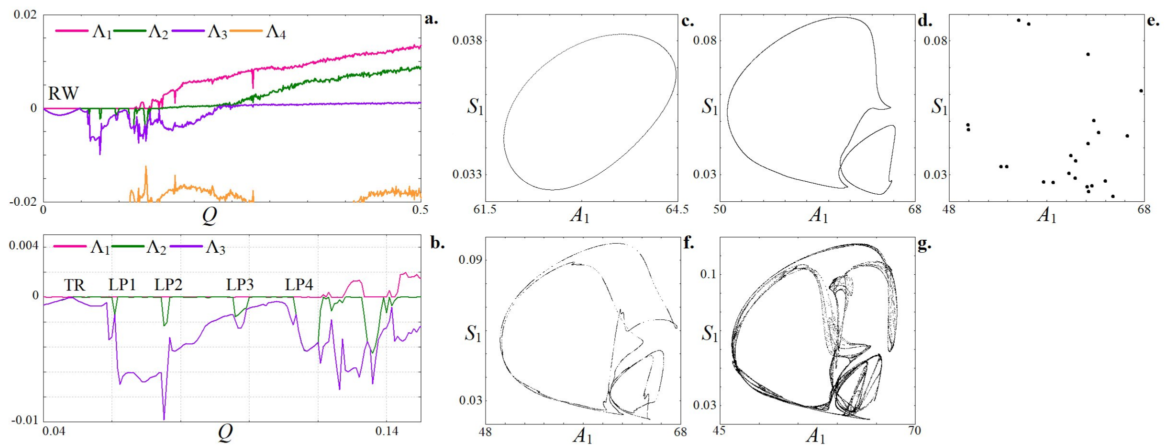

FIG. 6. Illustrations of hyperchaos formation. **a.**, **b.** Plots of Lyapunov exponents versus the coupling strength, and Poincaré maps. $\alpha = 2777$, **c.** - $Q = 0.05$, **d.** - $Q = 0.11$, **e.** - $Q = 0.12$, **f.** - $Q = 0.121$, **g.** - $Q = 0.15$.

tive Lyapunov exponents.

After the torus destruction, the graphs of Lyapunov exponents show an interval $Q(0.23 - 0.26)$, within which the largest Lyapunov exponent is positive, the second and the third exponents are very close to zero. Within the specified interval, the second and third exponents fluctuate near zero value and at $Q \approx 0.26$ the third exponent becomes zero, and the second is positive. This interval corresponds to the region in the parameter plane where there are all three solutions discussed in Section III. The absorption of a saddle-focus cycle with a two-dimensional unstable manifold by a chaotic attractor can lead to the development of hyperchaos.

To test this hypothesis, the trajectories of the saddle cycles were extracted using their AUTO-continuations, their two-dimensional projections onto (A_1, S_1) plane in Poincaré sections were found and presented together with the maps of chaos in Figs. 7a-7c (colored dots).

We focus on the evolution of the fixed point for the cycle RW(9,2) which is expectedly more important for hyperchaos formation due to the two multipliers greater than one. As obvious from Fig. 7a, the chaotic attractor is distanced from the fixed point of the saddle-focus RW cycle for $Q = 0.2$ (green point). As the coupling increases, the chaotic attractor approaches this fixed point and merges with it at least in this plane. Note that the phase space is 12-dimensional and the results observed in two-dimensional Poincaré section should be supported by calculations in the full phase space. To be sure of approaching a chaotic attractor, we computed the minimum distance from the fixed point for RW(9,2) to the chaotic attractor in the full phase space. The values D_{SF} of the distances are presented in Table 1 together with the values Λ_i of the four largest Lyapunov exponents.

When the coupling strength Q changes from 0.2 to 0.2974, the distance from the chaotic attractor to the fixed point of saddle-focus cycle in the Poincaré map decreases from 15.876 to 1.627. Although the distance is not very close to zero,

Q	Λ_1	Λ_2	Λ_3	Λ_4	D_{SF}	D_{S1}
0.2	0.005	0.0	-0.003	-0.017	15.88	0.0
0.2295	0.006	0.0	-0.001	-0.019	10.80	0.046
0.2974	0.008	0.004	0.0	-0.022	1.63	0.207

TABLE I. The four largest Lyapunov exponents (Λ_i) and minimal distance from chaotic map to saddle-focus point (D_{SF}) and to 8D period-1 saddle point (D_{S1}).

this strong reduction in distance increases the probability of merging saddle-focus RW-cycle with chaos. Note that for calculation of the distance the RW(9,2) cycle time series is fixed as prescribed by the AUTO method. This may give the distance between the cycle and chaos slightly overestimated whereas the time series fluctuations of real RW(9,2) can overlap this gap. Such return times distributions are frequently used for estimating Lyapunov exponents and entropy of dynamical models[50] and also for detecting rare and extreme events[51].

The suggested merging may stimulate the appearance of unstable RW in hyperchaotic trajectories. Specific unstable periodic orbits (UPO) in 12-dimensional phase space are not easy to identify, but phase relations between RW variables of three oscillators and their amplitudes are rather different from those for chaotic regime, making it possible to distinguish them. Although the probability of RW formation is not large, these random UPOs are reliably observed near $Q = 0.27$ (see examples in Fig. 8a, 8b) whereas any similar parts are absent for coupling strength before chaos-hyperchaos transition.

Direct visualization of RW limit cycle elements can be supplemented by assessing the changes in return times distributions before and after chaos-hyperchaos transition at an appropriately chosen level of a Poincaré section. Such return times distributions are frequently used for the estimations of Lyapunov exponents and entropy of the dynamical models[52].

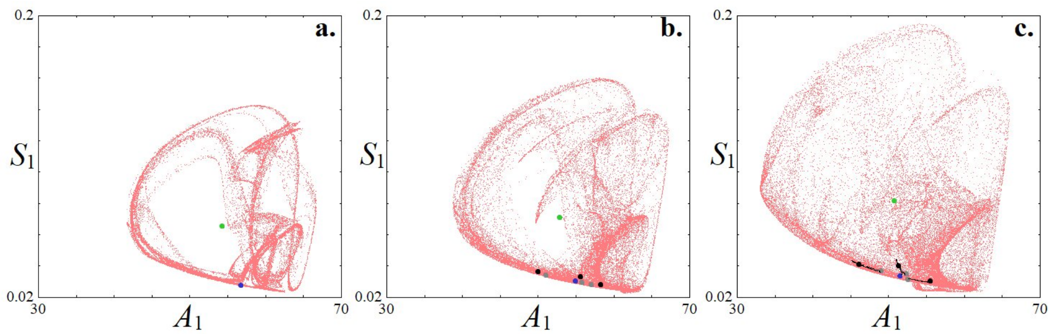

FIG. 7. The maps of chaos and the fixed points in Poincaré section for the limit cycles for **a.** $Q = 0.2$, **b.** $Q = 0.2294$, **c.** $Q = 0.2975$. Chaotic attractors are depicted by red color, saddle-focus RW(9,2) - green dot, 8D saddle cycle AS2in-1out(10,1) - blue dot, pair of 8D saddle cycles AS3^1 and AS3^2 - black and grey dots correspondingly.

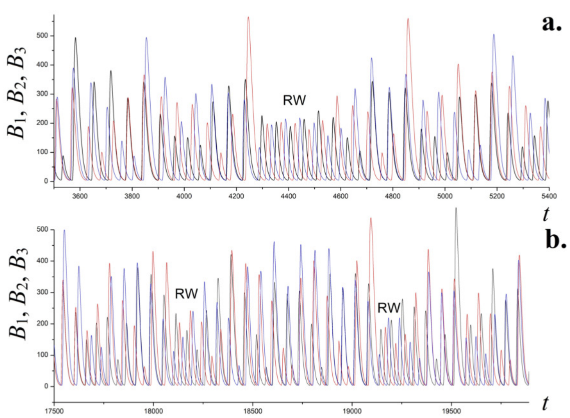

FIG. 8. Examples of random manifestation of unstable RW segments in time series of hyperchaotic attractor for **a.** $Q = 0.272$; **b.** Q=0.3.

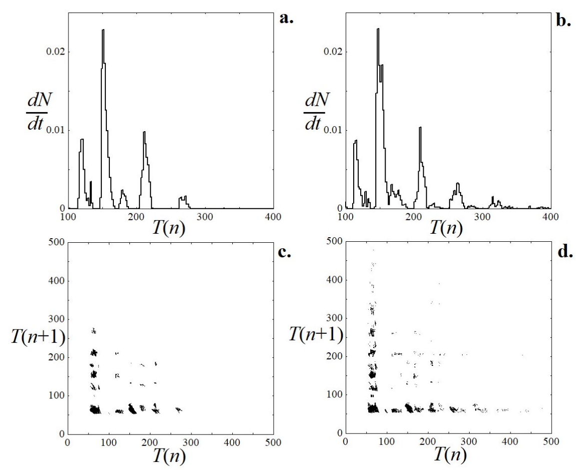

FIG. 9. The distributions of return times and the sequential period maps: **a.**, **c.** - $Q = 0.23$; **b.**, **d.** - $Q = 0.27$.

We build one-dimensional map using standard Poincaré section of variables B_i. The RW limit cycle is unstable but, as seen in Fig.8, fluctuations of B_i amplitudes are not large and limited compared with other oscillation maxima prompting to choose B_i-sections going slightly above the parts of the RW cycle. According to the examples in Fig. 8, the collection of return times calculated for the section of hyperchaotic time series at a level of $B_i = 230 - 240$ should contain the longest return times because this level is higher than RW amplitudes. To choose this level more accurate, the large number (20000) return times were calculated for $Q = 0.23$ that corresponds to chaotic attractor just before its transition to hyperchaos (Fig. 9a). We focus on the $T(n)$ distribution after $T(n)$=100 which shows the maximum $T(n)$ to be near $T(n)$=275.

The same calculations of $T(n)$ made after transition of the system to hyperchaos, e.g. for $Q = 0.27$, show a very similar distribution for $T(n) < 275$ and the robust presence of $T(n) > 310$ (Fig. 9b). The same changes of $T(n)$ are illustrated using sequential period maps in Fig. 9c, 9d. We argue that these rare long intervals are the manifestation of the longest RW pieces in hyperchaos because the return times generated by shorter RW pieces cannot be distinguished from those in chaos.

In addition to 12-dimemsional RW(9,2), we observed 8-dimensional period-3 limit cycle and its bifurcations up to a weak 8-dimensional chaos in the interval of Q between 0.2 and 0.345 (Fig. 4b) which overlaps with the area where chaos-hyperchaos transition takes place. Figure 7 shows the fixed points for these cycles with one-dimensional (black) and two-dimensional (gray) unstable manifolds. In the (S_1, A_1) projection these points touch the chaotic map, suggesting that the AS3(9,2) cycle may affect the hyperchaos formation. The existence of this cycle strongly requires that phase points and parameters for a pair of the oscillators be identical, which is very unlikely in 12-dimensional chaos. However, the presence of attractive manifolds can stimulate the appearance of very transient segments in time series which resemble 8-dimensional cycles. They are actually observed in the hyperchaotic trajectories for some pairs of variables. Nevertheless, they are too short to contribute into the hyperchaotic skeleton. The fixed point for 8-dimensional period-1 cycle AS2in-1out in Poincaré section (Fig. 7, blue) also touches the chaotic map. Segments of this cycle are observed in chaotic trajectories but the cycle has only one-dimensional unstable manifold that makes it nonmeaningful for hyperchaos formation.

We conclude that one of the reasons why hyperchaos arises is the merge of unstable cycle RW with chaos. At the moment, there is no evidence that two unstable 8-dimensional cycles participate in hyperchaos formation. A further study on the evolution of these asymmetric regimes over the (Q -α)-parameter plane will shed light on their stability and interactions with hyperchaos.

V. DISCUSSION

Most studies on the routes to hyperchaos in coupled oscillators explored models with chaotic dynamics, choosing diffusion in different versions for oscillator interaction. In contrast, in the ring Repressilator the limit cycle born at the Andronov-Hopf bifurcation does not undergo further bifurcations when control parameter α is growth. The main source of complex dynamics in Repressilator populations is the coupling scheme based on the bacterial quorum sensing mechanism. It means that all variables of Repressilators are strongly localized and their interactions are realized via diffusive mixing of special signal molecules in the mutual environment. The ring is composed of three genes, their promoters can independently control the production of signal molecules as well as the type of their activity creating different schemes of coupling. We used one design of QS-coupling which already demonstrated the generation of rich multistability in two coupled Repressilators[35–38]. Two Repressilators were shown to generate chaos via torus destruction, as well as via a period-doubling cascade of resonant cycles. Moreover, there are parameter intervals where these two chaotic regimes collide but we have never observed hyperchaos to appear.

Here we demonstrated numerically the presence of hyperchaos over wide parameter ranges (Fig. 1b) except for the small values of α. We already discussed in[39] the complex evolution of tori in three mean-field QS-coupled Repressilators for small α. In system (1) variables C_i are activated by variables S_i, the concentrations of which depend both on the values of B_i and on the processes of S_i mixing and dilution in the mean field. It means that, due to mixing, the C_i stimulation by S_i is significantly affected by three combinations of variables B_i, resulting in complex periodic activation of Repressilators, which is also coupling strength-dependent. For small Q the stable RW cycle dominates up to the Neimark-Sacker bifurcation (Fig. 2) leading to torus formation. In particular, for $\alpha = 2777$ we found successive formation of two tori (Fig. 6c, 6d) and the destruction of the last complex torus resulting in chaos formation (Fig. 6e). In turn, limit cycle RW(11,0) loses stability becoming saddle-focus cycle with two-dimensional unstable manifold, RW(9,2). Further merging of RW(9,2) with chaos results in continuous development of hyperchaos as coupling growth.

There are other studies with simple oscillators focused on the routes to hyperchaos. For example, Perlikovsy et al.[22] investigated a ring of unidirectionally diffusion coupled autonomous Duffing oscillators where each individual oscillator in the absence of coupling has only trivial equilibrium dynamics. With this coupling scheme, the birth of a limit cycle is observed, which gives rise to torus formation at Neimark-Sacker bifurcation. The torus undergoes complex evolution via torus doubling up to hyperchaos. Despite very different differential equations in this and our model (1), some events on the way to hyperchaos are similar.

Scenario for the route to hyperchaos principally different from that realized for coupled chaotic oscillators was found in the model of two anti-phase periodically excited Toda oscillators[16]. A single autonomous Toda oscillator is a dissipative model which, like Duffing's oscillator, manifests only stable steady state. A non-autonomous model can demonstrate oscillations and transition to chaos via period-doubling bifurcations. With increasing coupling strength hyperchaos is formed via a sequence of Neimark-Sacker bifurcations of resonant cycles and the absorption of saddle-focus cycles by the chaotic attractor.

The use of various forms of simple direct or conjugate diffusion to couple popular paradigmatic two-dimensional oscillators brought a lot of important results over several last decades. However, the spectrum of nonlinear systems is growing, many interesting systems are principally multidimensional and interactions between them cannot be reduced to simple diffusion. Our work demonstrates only one example of complex dynamics in three three-dimensional QS-coupled synthetic genetic oscillators. Certainly, the implication of other schemes of quorum sensing coupling in networks with other oscillators would discover new routes to diverse complex dynamics or, on the contrary, point out how to reach simple behavior.

ACKNOWLEDGEMENTS

This work is partially supported by a grant from the Russian Foundation for Basic Research (No. 19-02-00610) as well as the Government Assignment to the Lebedev Physical Institute (Project No. 0023-2019-0011). N. Stankevich acknowledges the Russian Foundation for Basic Research grant (No. 19-31-60030) for the partial funding support.

We thank A. Kazakov for interest to our work.

DATA AVAILABILITY

The data supporting numerical experiments presented in this paper are available from the corresponding author upon reasonable request.

[1] O. Rossler, "An equation for hyperchaos," Physics Letters A **71**, 155–157 (1979).

[2]S. Nikolov and S. Clodong, "Hyperchaos–chaos–hyperchaos transition in modified Rössler systems," Chaos, solitons & fractals **28**, 252–263 (2006).
[3]Y. Li, W. K. Tang, and G. Chen, "Hyperchaos evolved from the generalized Lorenz equation," International Journal of Circuit Theory and Applications **33**, 235–251 (2005).
[4]X. Wang and M. Wang, "A hyperchaos generated from Lorenz system," Physica A: Statistical Mechanics and its Applications **387**, 3751–3758 (2008).
[5]S. Pang and Y. Liu, "A new hyperchaotic system from the Lü system and its control," Journal of Computational and Applied Mathematics **235**, 2775–2789 (2011).
[6]S. Vaidyanathan, I. Moroz, A. Sambas, W. Sanjaya, *et al.*, "A new 4-d hyperchaotic two-wing system with a unique saddle-point equilibrium at the origin, its bifurcation analysis and circuit simulation," in *Journal of Physics: Conference Series*, Vol. 1477 (IOP Publishing, 2020) p. 022016.
[7]N. Stankevich, A. Kuznetsov, E. Popova, and E. Seleznev, "Chaos and hyperchaos via secondary Neimark–Sacker bifurcation in a model of radiophysical generator," Nonlinear dynamics **97**, 2355–2370 (2019).
[8]I. Sataev and N. Stankevich, "Cascade of torus birth bifurcations and inverse cascade of Shilnikov attractors merging at the threshold of hyperchaos," Chaos: An Interdisciplinary Journal of Nonlinear Science **31**, 023140 (2021).
[9]T. Kapitaniak and L. O. Chua, "Hyperchaotic attractors of unidirectionally-coupled Chuas circuits," International Journal of Bifurcation and Chaos **4**, 477–482 (1994).
[10]J. Rasmussen, E. Mosekilde, and C. Reick, "Bifurcations in two coupled Rössler systems," Mathematics and Computers in Simulation **40**, 247–270 (1996).
[11]D. Postnov, T. Vadivasova, O. Sosnovtseva, A. Balanov, V. Anishchenko, and E. Mosekilde, "Role of multistability in the transition to chaotic phase synchronization," Chaos: An Interdisciplinary Journal of Nonlinear Science **9**, 227–232 (1999).
[12]S. Yanchuk and T. Kapitaniak, "Symmetry-increasing bifurcation as a predictor of a chaos-hyperchaos transition in coupled systems," Physical Review E **64**, 056235 (2001).
[13]A. Čenys, A. Tamaševičius, A. Baziliauskas, R. Krivickas, and E. Lindberg, "Hyperchaos in coupled Colpitts oscillators," Chaos, Solitons & Fractals **17**, 349–353 (2003).
[14]B. Cannas and S. Cincotti, "Hyperchaotic behaviour of two bi-directionally coupled Chuas circuits," International Journal of Circuit Theory and Applications **30**, 625–637 (2002).
[15]T. Kapitaniak, K.-E. Thylwe, I. Cohen, and J. Wojewoda, "Chaos-hyperchaos transition," Chaos, Solitons & Fractals **5**, 2003–2011 (1995).
[16]N. V. Stankevich, A. Dvorak, V. Astakhov, P. Jaros, M. Kapitaniak, P. Perlikowski, and T. Kapitaniak, "Chaos and hyperchaos in coupled antiphase driven Toda oscillators," Regular and Chaotic Dynamics **23**, 120–126 (2018).
[17]V. Anishchenko and S. Nikolaev, "Generator of quasi-periodic oscillations featuring two-dimensional torus doubling bifurcations," Technical physics letters **31**, 853–855 (2005).
[18]I. R. Garashchuk, D. I. Sinelshchikov, A. O. Kazakov, and N. A. Kudryashov, "Hyperchaos and multistability in the model of two interacting microbubble contrast agents," Chaos: An Interdisciplinary Journal of Nonlinear Science **29**, 063131 (2019).
[19]I. Ovsyannikov and L. Shil'Nikov, "Systems with a homoclinic curve of multidimensional saddle-focus type, and spiral chaos," Mathematics of the USSR-Sbornik **73**, 415 (1992).
[20]L. P. Shilnikov and A. Shilnikov, "Shilnikov bifurcation," Scholarpedia **2**, 1891 (2007).
[21]A. Gonchenko, S. Gonchenko, A. Kazakov, and D. Turaev, "Simple scenarios of onset of chaos in three-dimensional maps," International Journal of Bifurcation and Chaos **24**, 1440005 (2014).
[22]P. Perlikowski, S. Yanchuk, M. Wolfrum, A. Stefanski, P. Mosiolek, and T. Kapitaniak, "Routes to complex dynamics in a ring of unidirectionally coupled systems," Chaos: An Interdisciplinary Journal of Nonlinear Science **20**, 013111 (2010).
[23]M. B. Elowitz and S. Leibler, "A synthetic oscillatory network of transcriptional regulators," Nature **403**, 335–338 (2000).
[24]H. Niederholtmeyer, Z. Z. Sun, Y. Hori, E. Yeung, A. Verpoorte, R. M. Murray, and S. J. Maerkl, "Rapid cell-free forward engineering of novel genetic ring oscillators," elife **4**, e09771 (2015).
[25]L. Potvin-Trottier, N. D. Lord, G. Vinnicombe, and J. Paulsson, "Synchronous long-term oscillations in a synthetic gene circuit," Nature **538**, 514–517 (2016).
[26]O. Boşe, A. Kuznetsov, and R. A. Pérez, "Existence of limit cycles in the repressilator equations," International Journal of Bifurcation and Chaos **19**, 4097–4106 (2009).
[27]S. Müller, J. Hofbauer, L. Endler, C. Flamm, S. Widder, and P. Schuster, "A generalized model of the repressilator," Journal of mathematical biology **53**, 905–937 (2006).
[28]D. McMillen, N. Kopell, J. Hasty, and J. Collins, "Synchronizing genetic relaxation oscillators by intercell signaling," Proceedings of the National Academy of Sciences **99**, 679–684 (2002).
[29]J. Garcia-Ojalvo, M. B. Elowitz, and S. H. Strogatz, "Modeling a synthetic multicellular clock: repressilators coupled by quorum sensing," Proceedings of the National Academy of Sciences **101**, 10955–10960 (2004).
[30]F. K. Balagaddé, H. Song, J. Ozaki, C. H. Collins, M. Barnet, F. H. Arnold, S. R. Quake, and L. You, "A synthetic escherichia coli predator–prey ecosystem," Molecular systems biology **4**, 187 (2008).
[31]L. You, R. S. Cox, R. Weiss, and F. H. Arnold, "Programmed population control by cell–cell communication and regulated killing," Nature **428**, 868–871 (2004).
[32]S. Hennig, G. Rödel, and K. Ostermann, "Artificial cell-cell communication as an emerging tool in synthetic biology applications," Journal of biological engineering **9**, 1–12 (2015).
[33]T. Danino, O. Mondragón-Palomino, L. Tsimring, and J. Hasty, "A synchronized quorum of genetic clocks," Nature **463**, 326–330 (2010).
[34]T. Zhou, J. Zhang, Z. Yuan, and L. Chen, "Synchronization of genetic oscillators," Chaos: An Interdisciplinary Journal of Nonlinear Science **18**, 037126 (2008).
[35]E. Ullner, A. Koseska, J. Kurths, E. Volkov, H. Kantz, and J. García-Ojalvo, "Multistability of synthetic genetic networks with repressive cell-to-cell communication," Physical Review E **78**, 031904 (2008).
[36]E. H. Hellen and E. Volkov, "Flexible dynamics of two quorum-sensing coupled repressilators," Physical Review E **95**, 022408 (2017).
[37]E. H. Hellen and E. Volkov, "How to couple identical ring oscillators to get quasiperiodicity, extended chaos, multistability, and the loss of symmetry," Communications in Nonlinear Science and Numerical Simulation **62**, 462–479 (2018).
[38]E. H. Hellen and E. Volkov, "Emergence of multistability and strongly asymmetric collective modes in two quorum sensing coupled identical ring oscillators," Chaos: An Interdisciplinary Journal of Nonlinear Science **30**, 121101 (2020).
[39]N. Stankevich and E. Volkov, "Evolution of quasiperiodicity in quorum-sensing coupled identical repressilators," Chaos: An Interdisciplinary Journal of Nonlinear Science **30**, 043122 (2020).
[40]I. Potapov, B. Zhurov, and E. Volkov, "Quorum sensing generated multistability and chaos in a synthetic genetic oscillator," Chaos: An Interdisciplinary Journal of Nonlinear Science **22**, 023117 (2012).
[41]E. Sánchez, D. Pazó, and M. A. Matías, "Experimental study of the transitions between synchronous chaos and a periodic rotating wave," Chaos: An Interdisciplinary Journal of Nonlinear Science **16**, 033122 (2006).
[42]G. Benettin, L. Galgani, A. Giorgilli, and J.-M. Strelcyn, "Lyapunov characteristic exponents for smooth dynamical systems and for Hamiltonian systems; a method for computing all of them. part 1: Theory," Meccanica **15**, 9–20 (1980).
[43]P. Ashwin, G. King, and J. W. Swift, "Three identical oscillators with symmetric coupling," Nonlinearity **3**, 585 (1990).
[44]M. Yoshimoto, K. Yoshikawa, and Y. Mori, "Coupling among three chemical oscillators: synchronization, phase death, and frustration," Physical Review E **47**, 864 (1993).
[45]E. I. Volkov and M. N. Stolyarov, "Temporal variability in a system of coupled mitotic timers," Biological cybernetics **71**, 451–459 (1994).
[46]D. Ruwisch, M. Bode, D. Volkov, and E. Volkov, "Collective modes of three coupled relaxation oscillators: the influence of detuning," International Journal of Bifurcation and Chaos **9**, 1969–1981 (1999).
[47]B. Ermentrout, *Simulating, analyzing, and animating dynamical systems: a guide to XPPAUT for researchers and students* (SIAM, 2002).
[48]V. Afraimovich and L. P. Shilnikov, "Invariant two-dimensional tori, their breakdown and stochasticity," Amer. Math. Soc. Transl **149**, 201–212

(1991).

[49] N. Stankevich, A. Kazakov, and E. Volkov, "Bistable tori and long transient dynamics in three coupled identical ring oscillators," in *2020 4th Scientific School on Dynamics of Complex Networks and their Application in Intellectual Robotics (DCNAIR)* (IEEE, 2020) pp. 238–241.

[50] E. Karatetskaia, A. Shykhmamedov, and A. Kazakov, "Shilnikov attractors in three-dimensional orientation-reversing maps," Chaos: An Interdisciplinary Journal of Nonlinear Science **31**, 011102 (2021).

[51] A. Mishra, S. Leo Kingston, C. Hens, T. Kapitaniak, U. Feudel, and S. K. Dana, "Routes to extreme events in dynamical systems: Dynamical and statistical characteristics," Chaos: An Interdisciplinary Journal of Nonlinear Science **30**, 063114 (2020).

[52] V. S. Anishchenko and S. V. Astakhov, "Poincaré recurrence theory and its applications to nonlinear physics," Physics-Uspekhi **56**, 955 (2013).